Proper orthogonal decomposition and recent advanced topics in wind engineering

Le Thai Hoa[*]

College of Technology, Vietnam National University, Hanoi
144 Xuan Thuy, Cau Giay, Hanoi, Vietnam

Abstract. Proper Orthogonal Decomposition and its Proper Transformations has been applied widely in many engineering topics including the wind engineering recently due to its advantage of optimum approximation of multi-variate random fields using the modal decomposition and limited number of dominantly orthogonal eigenvectors. This paper will present fundamentals of the Proper Orthogonal Decomposition and its Proper Transformations in both the time domain and the frequency domain based on both covariances matrix and cross spectral matrix branches. Moreover, the most recent topics and applications of the Proper Orthogonal Decomposition and its Proper Transformation in the wind engineering will be emphasized and discussed in this paper as follows: (1) Analysis and synthesis, identification of the multi-variate dynamic pressure fields; (2) Digital simulation of the multi-variate random turbulent wind fields and (3) Stochastic response prediction of structures due to the turbulent wind flows. All applications of the Proper Orthogonal Decomposition and its Proper Transformations will be investigated under numerical examples, especially will be formulated in both time domain and the frequency domain.

Keywords: Proper Orthogonal Decomposition, Proper Transformation, wind engineering, unsteady pressure fields, turbulence simulation, stochastic response.

1. Introduction

Proper Orthogonal Decomposition (POD), also known as Karhunen-Loeve Decomposition [1,2], has been applied in many engineering fields such as the random fields, the stochastic methods, the image processing, the data compression, the system identification and control and so on [3-5]. In the wind engineering, the POD has been used in the most recent topics as follows: i) Stochastic decomposition and order-reduced modeling of multi-variate random fields (turbulent wind, pressures and forces) [6-10]; ii) Representation and simulation of multi-variate random turbulent wind fields [11-14] and iii) Stochastic response prediction of structures in the turbulent wind fields [15-18]. The POD has been applied to optimally approximate the multi-variate random fields through use of low-order orthogonal vectors from modal decomposition of either zero-time-lag covariance matrix or cross spectral density one of this multi-variate random field. According to type of basic matrix in the modal

---
[*] Tel.: 84-4-3754.9667
E-mail: thlc@vnu.edu.vn

decomposition, the POD has been branched by either the Covariance Proper Transformation or the Spectral Proper Transformation. Main advantage of the POD is that the multi-variate random fields can be decomposed and described in such simplified way as a combination of a few low-order dominant eigenvectors (modes) and omitting higher-order ones that is convenient for order-reduced representation of the random fields, random force modeling and stochastic response prediction.

Up to now, the covariance matrix-branched POD and its transformation have been applied favorably for analysis and synthesis of the random field, especially of dynamic surface pressure field around low-rise and tall buildings as well as bridge girders [6-10] due to its straightforward in computation and interpretation. Because low-order modes contribute dominantly to total energy of the random fields and their energy proportions reduce very fast with respect to an increase of mode order, thus it is reasonable to thing that these low-order modes can represent and interpret to any physical cause occurring on physical models. Some authors used the POD to analyze random pressure field and to find out relation between pressure field-based covariance modes and physical causes, however, discussed that in many cases that consistent linkage between dominant covariance modes and physical causes may be fictitious [6,7,10]. Many effects such as number of pressure positions, pressure position arrangement, and presence of mean pressure values and so on can influence sensitively to resulting covariance modes [10]. Spectral matrix-based application to decompose the random field is rare due to its complexities in computation and interpretation, but it is promising due to its complete decoupling solution at every frequency, consequently decoupling in the time domain including zero-time-lag condition. De Grenet and Ricciardelli [19] discussed in using the Spectral Proper Transformation to study the fluctuating pressure fields around squared cylinder and boxed girder.

Representation and simulation of the multi-variate random turbulent fields surrounding structures is required for evaluating the induced forces and the random response of structures due to the turbulent winds in the time domain. Spectral representation methods basing on the cross spectral density matrix have been applied almost so far due to availability of the auto power spectral densities of turbulent components. These simulation methods, moreover, depend on decomposition techniques of this cross spectral density matrix through either the Cholesky's decomposition [20,21] or the modal decomposition [11-14]. In the former, the cross spectral density matrix is decomposed by product of two lower and upper triangular matrices, whereas the modal decomposition uses spectral eigenvectors (spectral modes) and spectral eigenvalues obtained from the spectral matrix-branched POD in the later. Main advantage of using the Spectral Proper Transformation in simulating the multi-variate random turbulent wind field is that only little number of the low-order dominant spectral modes and associated spectral eigenvalues is accuracy enough for whole simulating process. Moreover, the low-order spectral modes and spectral eigenvalues also contain their physical significance of the multi-variate random turbulent wind field.

Random response prediction of structures due to the turbulent wind forces usually burdens a lot of computational difficulties due to projection of the full-scale induced forces on generalized structural coordinates. As a principle, the multi-degree-of-freedom motion equations of structures are decoupled into the generalized coordinates and the structural modes due to the structural modal transformation. Conventional methods of the gust response prediction of structures has used concept of the Joint Acceptance Function to decompose the full-scale turbulent-induced forces, then to be associated with the generalized structural coordinates. New approach of the random response prediction of structures due to the turbulent wind flows has been proposed recently with concept of the Double Modal Transformations, in which the structural modes are associated with turbulent-induced loading modes that are decomposed by the Proper Transformations in order to determine the random response of structures. The Spectral Proper Transformation has been applied for the response prediction in the frequency domain of simple frame [15], buildings [16], bridges [17], especially, its application of the

Covariance Proper Transformation for the random response of bridges has discussed by Le and Nguyen [14,18].

This paper aims to present fundamentals of the POD, its Proper Transformations in both the covariance and spectral matrix branches with emphasis on recent advanced topics in the wind engineering: (1) Analyzing, identifying and reconstructing the random surface pressure fields around some typical rectangular cylinders, moreover, important role of the first mode including relationship with physical phenomena; (2) Simulating the multi-variate spatially-correlated random turbulent field with effect of the spectral modes; (3) Predicting the stochastic response of structures in the frequency domain and in the time domain. These applications will be presented with examples and discussions.

2. Proper orthogonal decomposition and its proper transformations

2.1. Proper orthogonal decomposition

The Proper Orthogonal Decomposition is considered as optimum approximation of the multi-variate random field in which a set of orthogonal basic vectors is found out in order to expand the random process into a sum of products of these time-independent basic orthogonal vectors and time-dependant uncorrelated random processes. Let consider the multi-variate correlated random process at N--node field containing correlated N-subprocesses $v(t) = \{v_1(t), v_2(t), ..., v_N(t)\}^T$ is approximated as:

$$v(t) = x(t)^T \Theta = \sum_{i=1}^{N} x_i(t)\theta_i \qquad (1)$$

where $x(t)$: time-dependant uncorrelated random process (also called as principal coordinates) $x(t) = \{x_1(t), x_2(t), ..., x_N(t)\}^T$; Θ : time-independent orthogonal modal matrix $\Theta = [\theta_1, \theta_2, ..., \theta_N]^T$.

Mathematical expression of optimality is to find out the orthogonal modal matrix in order to maximize the projection of the multi-variate correlated random process onto this modal matrix, normalized due to the mean square basis [1,2]:

$$Max \frac{\langle |(v(t) \otimes \Theta)|^2 \rangle}{\|\Theta\|^2} \qquad (2)$$

where $(\otimes), \langle . \rangle, |.|, \|.\|$ denote to inner product, expectation, absolute and Euclidean squared norm operators, respectively.

Optimum approximation of the random process in Eq.(1) using the shape function matrix defined in Eq.(2) is known as the Karhunen-Loeve decomposition. It is proved that the shape function matrix in this optimality can be found out as eigenvector solution of eigen problem from basic matrix that are either zero-time-lag covariance matrix or cross spectral density matrix formed by the multi-variate correlated random process. It is also notable that eigenvalues gained from this eigen solution usually reduce fast, accordingly, only very few number of low-order eigenvectors associated with low-order high eigenvalues can obtain the optimum approximation and simplified description of the random fields.

2.2. Matrix representation of multi-variate random fields

Zero-time-lag covariance matrix and cross power spectrum density matrix are commonly used to

characterize for the multi-variate correlated random process in the time domain and in the frequency one, which are determined as follows:

$$R_v = [R_{u_k u_l}(0)] = \begin{bmatrix} R_{u_1 u_1}(0) & R_{u_1 u_2}(0) & \cdots & R_{u_1 v_N}(0) \\ R_{u_2 u_1}(0) & R_{u_2 u_2}(0) & \cdots & R_{u_2 v_N}(0) \\ \vdots & \vdots & \ddots & \vdots \\ R_{v_N u_1}(0) & R_{v_N u_2}(0) & \cdots & R_{v_N v_N}(0) \end{bmatrix} ; S_v = [S_{u_k u_l}(n)] = \begin{bmatrix} S_{u_1 u_1}(n) & S_{u_1 u_2}(n) & \cdots & S_{u_1 v_N}(n) \\ S_{u_2 u_1}(n) & S_{u_2 u_2}(n) & \cdots & S_{u_2 v_N}(n) \\ \vdots & \vdots & \ddots & \vdots \\ S_{v_N u_1}(n) & S_{v_N u_2}(n) & \cdots & S_{v_N v_N}(n) \end{bmatrix} \quad (3)$$

where R_v, S_v: zero-time-lag covariance and cross spectral matrices respectively; $R_{v_k v_l}(0), S_{v_k v_l}(m)$: elements of the covariance matrix and the cross power spectral one between $v_k(t)$ and $v_l(t)$ at nodes k, l, are determined as follows:

$$R_{v_k v_l}(0) = E[v_k(t)v_l^T(t)]; \quad S_{v_k v_l}(n) = \sqrt{S_{v_k v_k}(n)S_{v_l v_l}(n)}COH_{v_k v_l}(n, \Delta_{kl}) \quad (4)$$

where E[],T denote to the expectation and transpose operators; n: frequency variable; $S_{v_k v_k}(n), S_{v_l v_l}(m)$: auto power spectral densities of $v_k(t)$ and $v_l(t)$; $COH_{v_k v_l}(n, \Delta_{kl})$: coherence function between two separated nodes k, l accounting for spatial correlation of the random sub-processes in the frequency domain which can be determined by either empirical model or physical measurement.

It is noted that the zero-time-lag covariance matrix is symmetric, real and positive definite, whereas the cross spectral one is symmetric, real (because the quadrature spectrum has been neglected) and Hermittian semi-positive definite at each frequency.

2.3. Covariance proper transformation

The covariance matrix-based orthogonal vectors are found as the eigenvector solution of the eigen problem of the zero-time-lag covariance matrix $R_v(0)$ of the N-variate correlated random process $v(t)$:

$$R_v \Theta_v = \Gamma_v \Theta_v \quad (5)$$

where Γ_v, Θ: covariance matrix-based eigenvalue and eigenvector matrices $\Gamma_v = diag(\gamma_{v1}, \gamma_{v2} \cdots \gamma_{vN})$, $\Theta_v = [\theta_{v1}, \theta_{v2} \cdots \theta_{vN}]$, respectively. Due to symmetric, real, positive-definite covariance matrix, thus the covariance eigenvalues are real and positive, and the covariance eigenvectors (also called as covariance modes) are also real, satisfy the orthogonal conditions:

$$\Theta_v \Theta_v^T = I; \quad \Theta_v R_v \Theta_v^T = \Gamma_v \quad (6)$$

Then, the multi-variate correlated random process and its covariance matrix can be reconstructed approximately using j-order truncated number of low-order eigenvalues, eigenvectors as follows:

$$v(t) = \Theta_v x_v(t) \approx \sum_{j=1}^{\tilde{N}} \theta_{v_j} x_{v_j}(t) ; R_v = \Theta_v \Gamma_v \Theta_v^T \approx \sum_{j=1}^{\tilde{N}} \theta_{v_j} \gamma_{v_j} \theta_{v_j}^T \quad (7)$$

where $x_v(t) = \{x_{v_1}(t), x_{v_2}(t), \cdots, x_{v_N}\}^T$: low-order covariance principal coordinates as uncorrelated random subprocesses; $\tilde{N}$: number of truncated covariance modes ($\tilde{N} \ll N$). Expressions in Eq.(7) is also known as the Covariance Proper Transformation.

Covariance principal coordinates can be determined from observed data as follows:

$$x_v(t) = \Theta_v^{-1} v(t) = v(t)\Theta_v = \sum_{j=1}^{N} v_j(t)\theta_{v_j} \quad (8)$$

If the random field contains the zero-mean subprocesses, furthermore, the covariance principal coordinates also are zero-mean uncorrelated random subprocesses, satisfy some characteristics:

$$E[x_{v_k}(t)] = 0; \quad E[x_{v_k}(t)x_{v_l}(t)^T] = \gamma_{v_k}\delta_{kl}$$ (9)

Where δ_{kl} : Kronecker delta.

2.4. Spectral proper transformation

The spectral matrix-based orthogonal vectors are found as eigenvector solution of the eigen problem from the cross spectral density matrix $S_v(n)$ of the N-variate correlated random process $v(t)$:

$$S_v(n)\Psi_v(n) = \Lambda_v(n)\Psi_v(n)$$ (10)

where $\Lambda_v(n), \Psi_v(n)$: spectral eigenvalue and eigenvector matrices $\Lambda_v(n) = diag(\lambda_{v1}(n),\lambda_{v2}(n),...\lambda_{vN}(n))$,
$\Psi_v(n) = [\psi_{v1}(n),\psi_{v2}(n),...\psi_{vN}(n)]$, respectively. It is noted that the spectral eigenvalues are real and positive, whereas the spectral eigenvectors (spectral modes) are generally complex, however, if the cross spectral matrix is real then spectral modes are also real ones. The spectral eigenvalues and the spectral modes satisfy such orthogonal conditions as follows:

$$\Psi_v^{*T}(n)\Psi_v(n) = I; \quad \Psi_v^{*T}(n)S_v(n)\Psi_v(n) = \Lambda_v(n)$$ (11)

Accordingly, the Fourier transform and the cross spectral density matrix of random process $v(t)$ can be represented approximately due to terms of the spectral eigenvalues and eigenvectors as follows:

$$\hat{v}(n) = \Psi_v(n)\hat{y}_v(n) \approx \sum_{j=1}^{\hat{N}}\psi_{v_j}(n)\hat{y}_{v_j}(n); \quad S_v(n) = \Psi_v(n)\Lambda_v(n)\Psi_v^{*T}(n) \approx \sum_{j=1}^{\hat{N}}\psi_{v_j}(n)\lambda_{v_j}(n)\psi_{v_j}^{*T}(n)$$ (12)

where $\hat{v}(n)$: Fourier transform of the random process $v(t)$; $\hat{y}_v(n)$: spectral principal coordinates as Fourier transform of uncorrelated random subprocesses $y_v(t) = \{y_{v_1}(t), y_{v_2}(t),...., y_{v_N}\}^T$; $\hat{N}$: number of truncated spectral modes ($\hat{N} \ll N$); * denotes to complex conjugate operator. Frequency-domain optimum approximation in Eq.(13) is also known as the Spectral Proper Transformation.

The spectral principal coordinates have some characteristics as follows:

$$E[\hat{y}_{v_k}(n)\hat{y}_{v_l}(n)^T] = \lambda_{v_k}(n)\delta_{kl}$$ (13)

3. Analysis and synthesis, identification of multi-variate dynamic pressure fields

In this application, multi-variate dynamic pressure field around some rectangular sections have been analyzed in the time domain and the frequency one using both the Covariance and Spectral Proper Transformations. Next, synthesis and identification of these originally pressure fields using few low-order covariance and spectral modes as well as linkage between these low-order modes and physical phenomena on the rectangular sections have been discussed. The dynamic pressure data have been directly measured in the wind tunnel.

3.1. Wind tunnel measurements of dynamic pressure

Pressure measurements have been carried out on three typical rectangular models with side ratios B/D=1, B/D=1 with splitter plate and B/D=5 in the wind tunnel. Pressure taps are arranged in chordwise directions labeled from position 1 to position 10 (model B/D=1) and from position 1 to position 19 (model B/D=5) (see Figure 1). Artificial turbulent flows are generated by grid device at mean wind velocities 3m/s, 6m/s and 9m/s corresponding to intensities of turbulence as I_u=11.46%,

I_w=11.23%; I_u=10.54%, I_w=9.28% and I_u=9.52%, I_w=6.65%, respectively. Dynamic surface pressures are simultaneously measured by the multi-channel pressure measurement system (ZOC23, Ohte Giken, Inc.), then discretized by A/D converter (Thinknet DF3422, Pavec Co., Ltd.) with sampling frequency at 1000Hz in 100 seconds. Normalized mean pressures and normalized root-mean-square fluctuating pressures can be determined from measured unsteady pressures as follows:

$$C_{p,mean}^{(i)} = \overline{p}^{(i)} / (0.5\rho U^2); \quad C_{p,rms}^{(i)} = \sigma_p^{(i)} / (0.5\rho U^2) \tag{14}$$

where i: index of pressure positions; $0.5\rho U^2$: dynamic pressure; $\overline{p}, \sigma_p$: mean value, standard deviation of unsteady pressure, respectively.
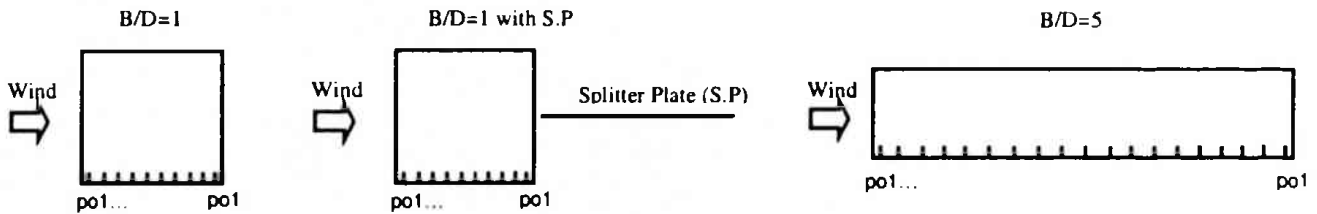
Fig. 1. Experimental models and pressure tap layouts.

It is previously clarified about bluff-body flow pattern around these sections that in the model B/D=1 it is favorable condition for the Karman vortices occur frequently at the wake of model; these Karman vortices are suppressed thanks to presence of splitter plate, whereas the bluff-body flow exhibits complex presence of separation bubble, reattachment, vortex shedding in the B/D=5 model.

3.2. Covariance proper transformation-based analysis

Eigenvalues and eigenvectors have been determined due to the eigen solution from the covariance matrix of the dynamic pressure fields. Energy contribution of the first covariance modes contribute respectively 76.92%, 65.29%, 43.77% to total energy of the system corresponding to models B/D=1 with the splitter plate, B/D=1 without the splitter plate and model B/D=5. Then, the covariance principal coordinates are computed using measured pressure data.
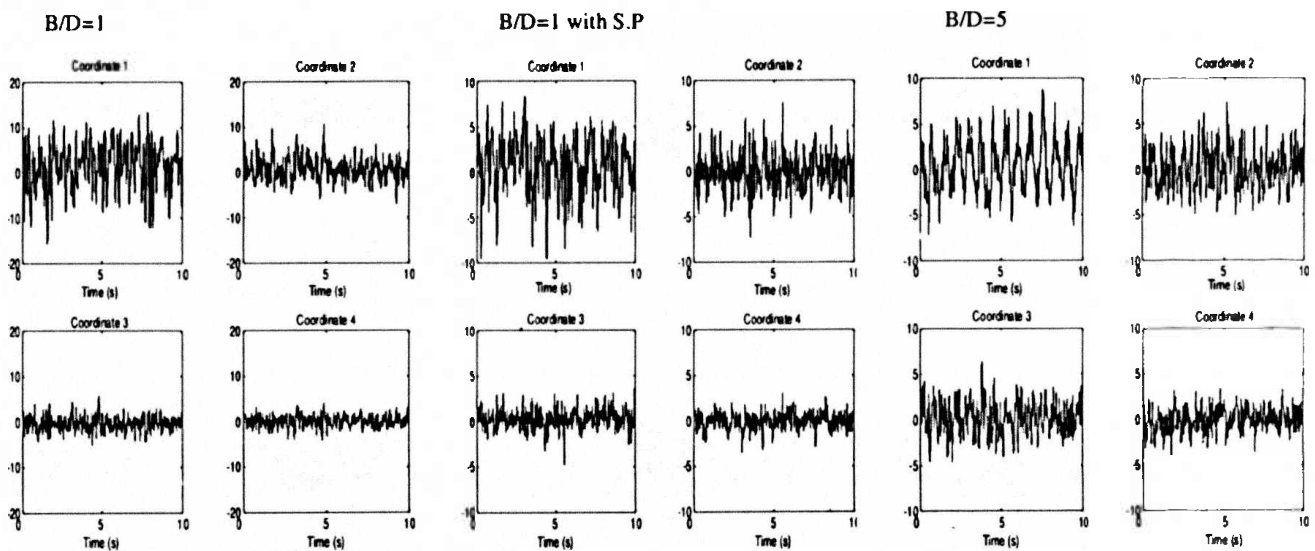

Fig. 2. First four principal coordinates (I_u=11.46%, I_w=11.23%).

Figure 2 shows first four uncorrelated principal coordinates of the three models associated with the covariance modes, whereas Figure 3 indicates power spectral densities of their corresponding principal coordinates. It is noteworthy that first coordinates not only dominate in the power spectrum but contain frequency characteristics of the random pressure field, whereas the other coordinates do not contain these frequencies.
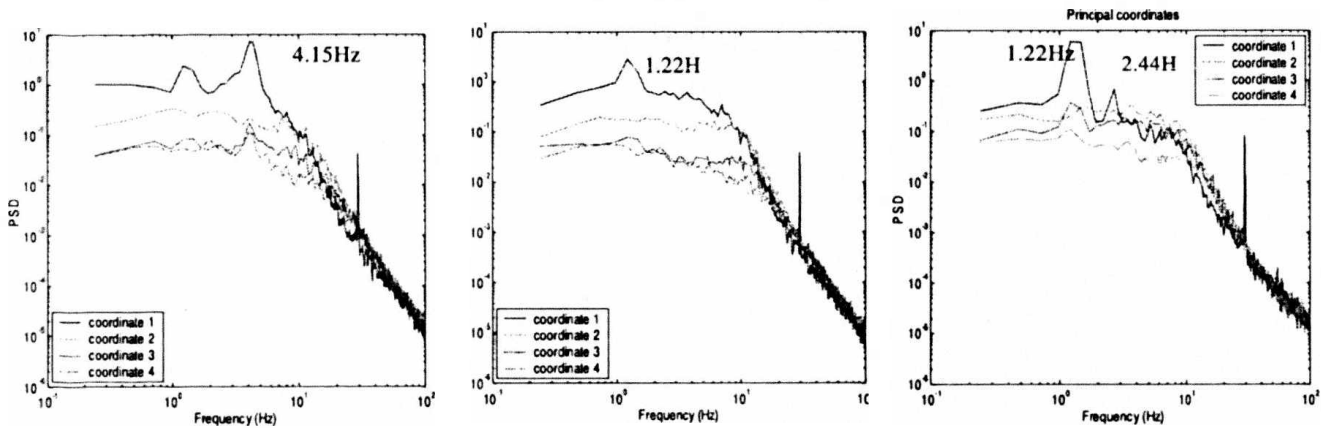

Fig. 3. Power spectra of first four principal coordinates (I_u=11.46%, I_w=11.23%).

Thus, it is discussed that the first covariance modes and associated principal coordinate play very important role in the identification and order-reduced reconstruction of the random pressure field due to their dominant energy contribution and frequency containing of physical phenomena.

3.3. Spectral proper transformation-based analysis

Spectral eigenvalues and eigenvectors have been obtained from the cross spectral matrix of the observed fluctuating pressure field. Figure 4 shows first five spectral eigenvalues on frequency band 0÷50Hz at the flow case 1. As seen that all first spectral eigenvalues from three models exhibit much dominantly than the other, especially theses first eigenvalues also contain characteristic frequency peaks of the pressure fields, whereas the other does not hold theses peaks. The first three spectral modes (eigenvectors) of the fluctuating pressure fields of the three models in the flow case 1 are shown in Figure 5.
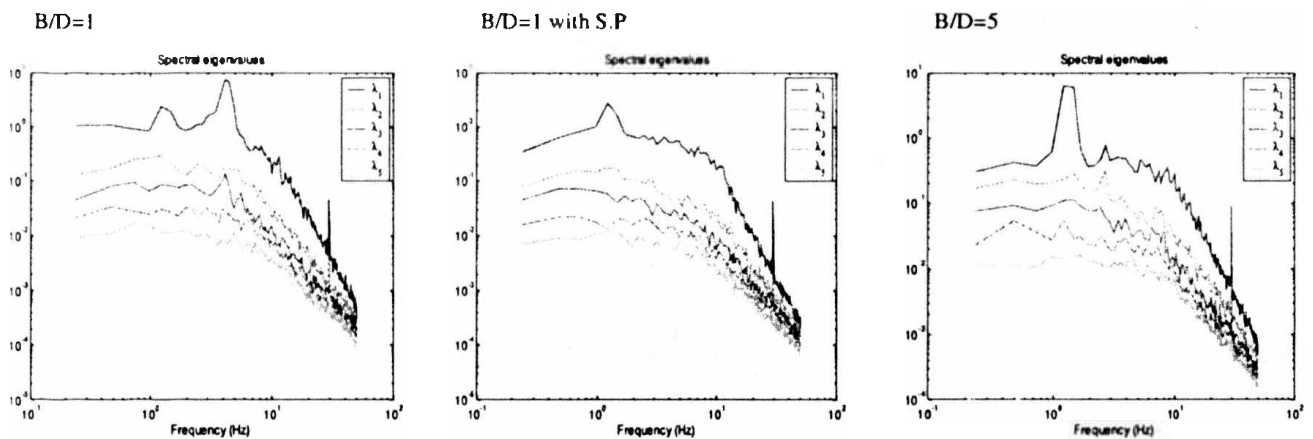

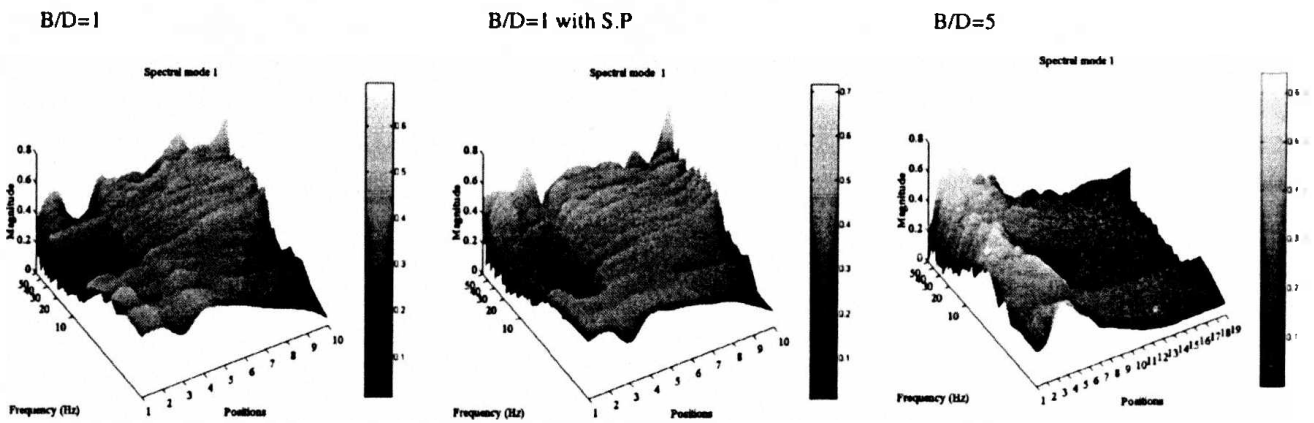Fig. 4. First five spectral eigenvalues of experimental models (I_u=11.46%, I_w=11.23%).

Fig. 5. First three spectral modes of experimental models (I_u=11.46%, I_w=11.23%).

Energy contributions of the spectral modes are estimated with cut-off frequency 50Hz. Similar to the covariance modes, the first spectral modes contain dominantly the system energy, for example, the first mode contribute 86.04%, 81.30%, 74.77%, respectively on total energy (I_u=11.46%, I_w=11.23%). In comparison with the covariance modes, it clearly observed that the first spectral modes are better solution than the first covariance one due to higher energy contribution.

It is argued that the first spectral mode and associated spectral eigenvalue play very important role in the identification and order-reduced reconstruction of the observed pressure fields due to their dominance in the energy contribution and containing of characteristic frequencies of the physical phenomena.

4. Digital simulation of multi-variate random turbulent wind field

4.1. Spectral representation method

Digital simulation of the multi-variate random turbulent wind fields using the Spectral Representation Method is widely used so far and will be presented here, in which the cross spectral matrix is decomposed by the Proper Spectral Transformation. Accordingly, the N-variate random turbulent process $v(t) = \{v_1(t), v_2(t), ..., v_N(t)\}^T$ can be represented [11-14]:

$$v(t) = \int_{-\infty}^{\infty} \exp(i2\pi nt)dB_v(n) \tag{15}$$

where $B_v(n) = \{B_{v_1}(n), B_{v_2}(n), ..., B_{v_N}(n)\}$: mean-zero uncorrelated orthogonal increment process satisfying as $E[dB_{v_i}(n)] = 0$, $dB_{v_i}(n) = dB_{v_i}(n)^*$, $E[dB_{v_i}(n_m)dB_{v_j}(n_k)^{*T}] = \delta_{ij}\delta_{mk}S_v(n)dn$; $S_v(n)$: cross spectral matrix.

Using the Spectral Proper Transformation to decompose and approximate the cross spectral matrix $S_v(n) = \sum_{j=1}^{N} S_{Y_j}(n) = \Psi_v(n)\Lambda_v(n)\Psi_v^{*T}(n) \approx \sum_{j=1}^{\hat{N}} \psi_{v_j}(n)\lambda_{v_j}(n)\psi_{v_j}^{*T}(n)$, the multi-variate random turbulent process can be decomposed and approximated by $\hat{N}$ summation of N-variate independent orthogonal processes:

$$v(t) = \sum_{j=1}^{\hat{N}} Y_{v_j}(t) = \sum_{j=1}^{\hat{N}} \left(\int_{-\infty}^{\infty} \psi_{v_j}(n)\sqrt{\lambda_{v_j}(n)} \exp(i2\pi n t)dn \right) \tag{16}$$

Subprocesses of the N-variate random turbulent process $v(t)$ can be simulated in the discrete frequency domain as:

$$v_i(t) = 2\sum_{j=1}^{\hat{N}} \sum_{l=1}^{\bar{N}} \psi_{v_j}(n_l)\sqrt{\lambda_{v_j}(n_l)} \exp(i2\pi n_l t)\Delta n_l \tag{17}$$

where i: index of simulated subprocess; j: index of spectral modes; l: index of frequency points; n_l: frequency value at moving point l; $\bar{N}$: number of frequency intervals; n_l: frequency interval at point l.

If the frequency domain is discretized constantly at every frequency interval Δn, then the Eq.(17) can be expanded:

$$v_i(t) = 2\sqrt{\Delta n}\sum_{j=1}^{\hat{N}} \sum_{l=1}^{\bar{N}} \psi_{v_j}(n_l)\sqrt{\lambda_{v_j}(n_l)} \cos(2\pi n_l t + \theta_{v_j}(n_l) + \phi_l) \tag{18}$$

where Δn_l: frequency interval at point l; Δn: constantly frequency interval $\Delta n = n_{up} / \bar{N}$ and $n_l = (l-1)\Delta n$, n_{up}: upper cut-off frequency; $\theta_{v_j}(n_l)$: phase angle of complex eigenvector $\psi_{v_j}(n_l) = |\psi_{v_j}(n_l)|\exp(i\theta_{v_j}(n_l))$, determined as $\theta_{v_j}(n_l) = \tan^{-1}\left(\text{Im}(\psi_{v_j}(n_l))/\text{Re}(\psi_{v_j}(n_l))\right)$; ϕ_l: phase angle considered as random variable uniformly distributed over $[0,2\pi]$.

In many cases, the spectral eigenvectors are real due to auto spectral densities are real and positive, Eq.(18) can be simplified as follows:

$$v_i(t) = 2\sqrt{\Delta n}\sum_{j=1}^{\hat{N}} \sum_{l=1}^{\bar{N}} \psi_{v_j}(n_l)\sqrt{\lambda_{v_j}(n_l)} \cos(2\pi n_l t + \phi_l) \tag{19}$$

The phase angles can be randomly generated using the Monte Carlo technique.

4.2. Numerical example and discussions

The spectral proper transformation has been applied to simulate the two multi-variate correlated random turbulent processes at 30 discrete nodes along a bridge deck: $u(i) = \{u_1(t), u_2(t),...,u_{30}(t)\}^T$ & $w(t) = \{w_1(t), w_2(t),...,w_{30}(t)\}^T$. Sampling rate of simulated turbulent time series is 1000Hz for total time interval 100 seconds. The cross spectral density matrices of u-, w-turbulences have been formulated based on auto spectral densities and spanwise coherence function. Targeted auto power spectral densities of u-, w-components are used the Kaimail's and Panofsky's models as well as the coherence function between two separated nodes along bridge deck used by exponentially empirical model [22]:

$$S_{uu}(n) = \frac{200 f u_*^2}{n(1+50f)^{5/3}}, \quad S_{ww}(n) = \frac{3.36 f u_*^2}{n(1+10f^{5/3})} \tag{20a}$$

$$COH_{v_k v_l}(n, \Delta_{kl}) = \exp\left(-\frac{c_v n |y_k - y_l|}{0.5(U_k + U_l)}\right) \tag{20b}$$

where f: non-dimensional coordinates; u_*: friction velocity; U_k, U_l: mean velocities at two separated nodes k, l; c_v: decay factor, $c_u = 10, c_w = 6.5$ [16]; $\Delta_{kl} = |y_k - y_l|$: distance between two nodes; y_k, y_l: longitudinal coordinates.

Cross spectral matrices $S_u(n)$, $S_w(n)$ of two random turbulent processes u(t), w(t) at the 30 structural deck nodes have been formulated. Spectral matrix-based analysis has been carried out to find out pairs of the spectral eigenvectors (also called spectral turbulent modes) and associated spectral eigenvalues. Figure 6 shows the first five spectral eigenvalues $\lambda_1(n) \div \lambda_5(n)$ on frequency band 0.01÷10Hz. It is observed that the first spectral eigenvalue $\lambda_1(n)$ exhibits much higher than the others on the very low frequency band 0.01÷0.2Hz with the u-turbulence, 0.01÷0.5Hz with the w-turbulence, however, all spectral eigenvalues not to differ beyond these frequency thresholds. This implies that only first pair of the spectral eigenvalue and the spectral eigenvector seems to be enough for representing and simulating the whole turbulent fields at the very low frequency bands, however, many more pairs are required at higher frequency bands.
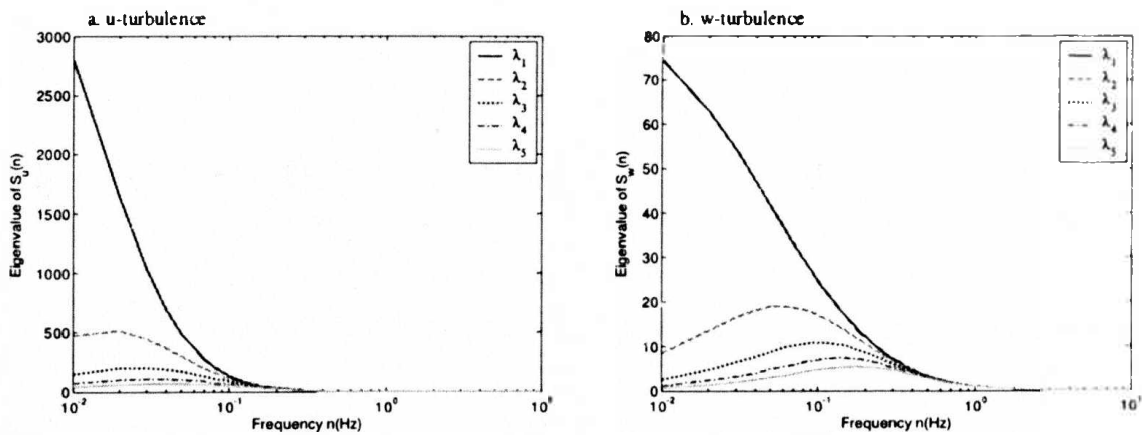

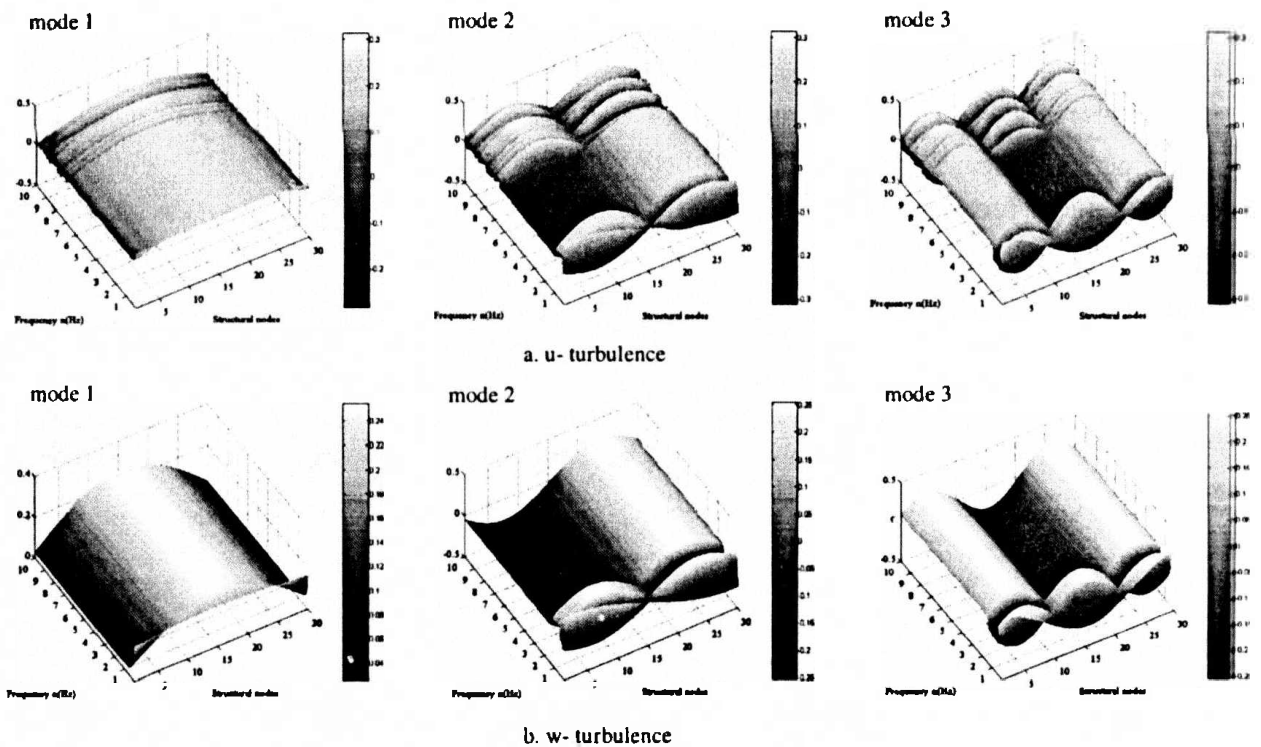Fig. 6. First five spectral eigenvalues: a. u-turbulence, b. w-turbulence.

a. u- turbulence

b. w- turbulence

Fig. 7. First three spectral turbulent modes: a. u-turbulence, b. w-turbulence.

The first three spectral turbulent modes $\psi_{v1}(n), \psi_{v2}(n), \psi_{v3}(n)$; $v = u, w$ on the same spectral band $0 \div 10$Hz is expressed in Figure 7. It can be seen from Figure 7 that the turbulent modes of u-,w-components look like as symmetrically and asymmetrically sinusoidal waves, in which number of wave halves increases incrementally with the order of eigenvectors.
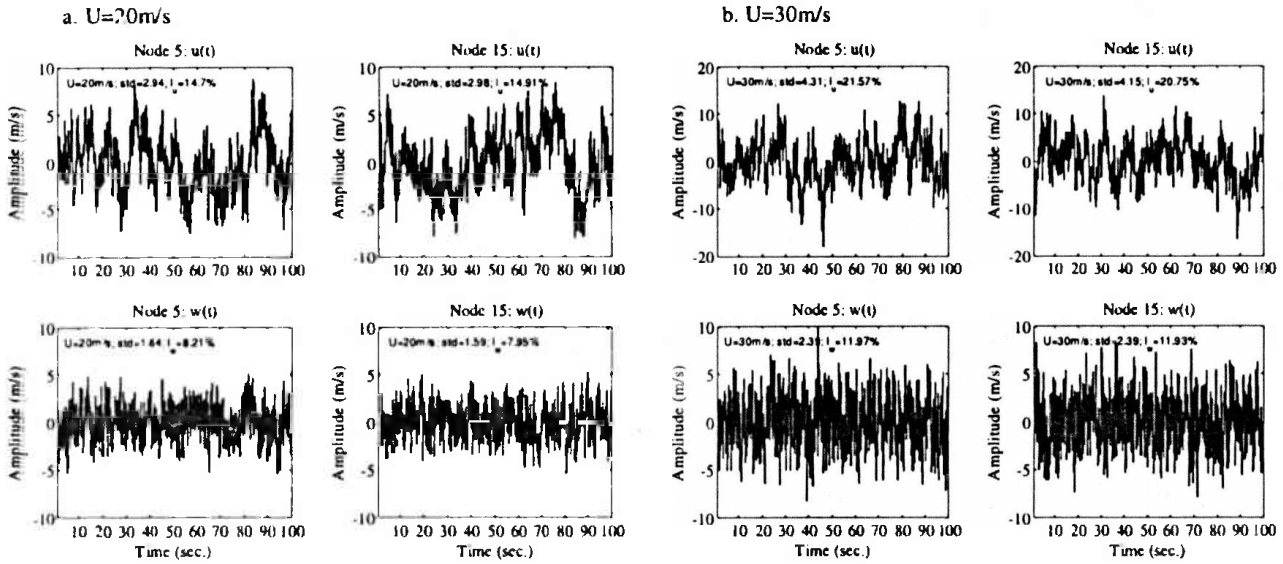

Fig. 8. Simulated time series in nodes 5&15: a. U=20m/s , b. U=30m/s.

Figure 8 shows simulated time series of two turbulent subprocesses at representative nodes 5 & 15 during 100-second interval at mean wind velocities 20m/s and 30m/s, respectively. Simulating time series of the random turbulent wind fields acting on discrete deck nodes are going to be used as input data to predict the random response of structure in the time domain in next application.

5. Random response prediction of structures in turbulence wind field

5.1. Structural modal transformation and turbulent-induced forces

Multi-degree-of-freedom motion equation of structures immersed in the atmospheric turbulent flow subjected to the turbulent-induced forces is expressed:

$$M\ddot{U}(t) + C\dot{U}(t) + KU(t) = F_b(t) \tag{21}$$

where M, C, K: globally mass, damping and stiffness matrices, respectively; $U, \dot{U}, \ddot{U}$: deflection vector and its derivative vectors; $F_b(t)$: turbulent-induced forces.

Transforming into generalized coordinates normalized by the mass matrix using $\overline{M}$ truncated low-order structural modes ($\overline{M} \ll M$, M: number of dynamic degree-of-freedom of structure), it satisfies:

$$U(t) = \Phi\xi(t) \approx \sum_{i=1}^{\overline{M}} \phi_i\xi_i(t) ; \Phi^T M\Phi = I ; \Phi^T C\Phi = \Xi ; \Phi^T K\Phi = \Omega \tag{22}$$

where ξ: generalized coordinate vector $\xi(t) = \{\xi_1(t), \xi_2(t), ..., \xi_M(t)\}^T$; Φ: modal matrix $\Phi = [\phi_1, \phi_2, ..., \phi_M]$; I: unit matrix; Ξ : diagonal damping matrix; Ω: diagonal stiffness matrix containing squared natural frequencies $\Omega = diag(\omega_1^2, \omega_2^2, ..., \omega_M^2)$.

Thus, single-degree-of-freedom motion equation in the i-th generalized coordinate excited by generalized turbulent-induced forces can be obtained:

$$\ddot{\xi}_i(t) + 2\zeta_i \omega_i \dot{\xi}_i(t) + \omega_i^2 \xi_i(t) = \phi_i^T F_b(t) \tag{23}$$

where ω_i, ζ_i : circular frequency and damping ratio, respectively.

Turbulent-induced forces lumped at discrete structural nodes are generated by laterally and vertically turbulent fluctuations u(t), w(t) which are considered as N-variate correlated random processes (N: number of structural nodes) as follows, see Figure 9:

$$u(t) = \{u_1(t), u_2(t), \dots, u_N(t)\}^T \; ; \; w(t) = \{w_1(t), w_2(t), \dots, w_N(t)\}^T \tag{24}$$
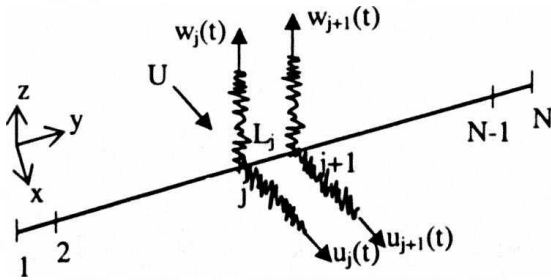

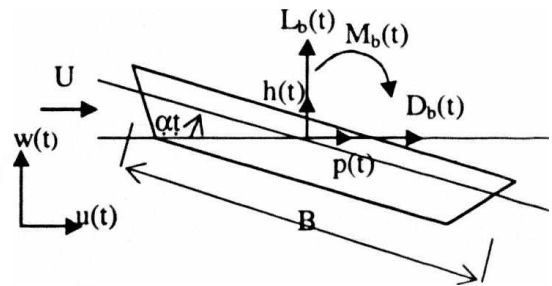Fig. 9. Turbulent loading processes.   Fig. 10. Turbulent-induced forces on section.

The uniform turbulent-induced forces are modeled due to quasi-steady theory corrected by frequency-dependant admittance functions as follows [22], see Figure 10:

$$L_b(t) = \frac{1}{2} \rho U^2 B [C_L \chi_{Lu}(n) \frac{2u(t)}{U} + (C_L' + C_D) \chi_{Lw}(n) \frac{w(t)}{U}] \tag{25a}$$

$$D_b(t) = \frac{1}{2} \rho U^2 B [C_D \chi_{Du}(n) \frac{2u(t)}{U} + (C_D' - C_L) \chi_{Dw}(n) \frac{w(t)}{U}] \tag{25b}$$

$$M_b(t) = \frac{1}{2} \rho U^2 B^2 [C_M \chi_{Mu}(n) \frac{2u(t)}{U} + C_M' \chi_{Mw}(n) \frac{w(t)}{U}] \tag{25c}$$

where C_L, C_D, C_M : aerodynamic coefficients at balanced angle of attack; C_L', C_D', C_M' : first-order derivatives with respect to angle of attack; ρ,B: air density and deck width; $\chi_{Fv}(F = L, D, M; v = u, w)$: aerodynamic transfer functions between turbulences and forces. Thus, the full-scaled global forces are obtained [14,18]:

$$F_b(t) = \frac{1}{2} \rho U B [C_u \chi_{Fu} u(t) + C_w \chi_{Fw} w(t)] \tag{26a}$$

$$F_b(t) = \begin{bmatrix} L_{bi}(t) \\ D_{bi}(t) \\ M_{bi}(t) \end{bmatrix}; C_u = \frac{1}{2} \rho U B \begin{bmatrix} 2C_L \overline{L} \\ 2C_D \overline{L} \\ 2BC_M \overline{L} \end{bmatrix}; C_w = \begin{bmatrix} C_L' \overline{L} \\ C_D' \overline{L} \\ BC_M' \overline{L} \end{bmatrix}; \overline{L} = diag(L_i); L_i = \begin{cases} 0.5 |y_2 - y_1|, & i = 1 \\ 0.5 |y_{i+1} - y_{i-1}|, 1 < i < N \\ 0.5 |y_N - y_{N-1}|, & i = N \end{cases} \tag{26b}$$

where C_u, C_w : full-scale force coefficient matrices; i: index of structural nodes

5..2. Spectral proper transformation-based formulation

Power spectra of the generalized responses can be obtained thanks to the second-order Fourier transform of Eq.(23) with the full-scale global forces Eqs.(26a),(26b) and optimum approximation from the Spectral Proper Transformation:

$$S_{\xi\xi}(n) = (\frac{1}{2}\rho UB)^2 \left[H(n)\Phi C_u^2 \Psi_u(n)\Lambda_u(n)\Psi_u^{*T}K(n)^2\Phi^T H(n)^{*T} + H(n)\Phi C_w^2\Psi_w(n)\Lambda_w(n)\Psi_w^{*T}K(n)^2\Phi^T H(n)^{*T} \right] \quad (27)$$

$$S_{\xi\xi}(n) = (\frac{1}{2}\rho UB)^2 \left[H(n)A_u(n)\Lambda_u(n)K(n)^2 A_u^{*T}(n)H^T(n) + H(n)A_w(n)\Lambda_w(n)K(n)^2 A_w^{*T}(n)H(n)^T \right] \quad (28)$$

where $A_u(n) = \sum_{j=1}^{\hat{N}} A_{u_{ij}}(n) = \sum_{j=1}^{\hat{N}} \phi_i^T C_u \psi_{u_j}(n)$; $A_w(n = \sum_{j=1}^{\hat{N}} A_{w_{ij}}(n) = \sum_{j=1}^{\hat{N}} \phi_i^T C_w \psi_{w_j}(n)$:cross modal factor

matrices accounting for interaction between spectral modes and structural ones; $H(n)$: frequency response function (FRF) matrix $H(n) = diag(|H_1(n)|,|H_2(n)|,... |H_{\bar{M}}(n)|)$ in which $|H_i(n)|$ denotes to FRF at natural frequency n_i; $K(n)^2$: squared aerodynamic admittance function.

Next, power spectra and root mean square (RMS) of the global responses can be estimated as follows:

$$S_U(n) = \Phi S_\xi(n)\Phi^T; \quad \sigma_U^2 = \int_0^\infty S_U(n)dn \quad (29)$$

where $S_U(n), \sigma_U^2$: spectra and root mean square of global responses, respectively.

Finally, global responses with respect to vertical, longitudinal and rotational directions can be combined from single-modal responses due to the principle of the squared root of the sum of the squares:

$$\sigma_r(n) = \sqrt{\sum_i^{\bar{M}_r} \sigma_{r,i}^2}; \quad r = h, p, a \quad (30)$$

where r denotes to displacement components: vertical (h), longitudinal (p), rotational (a); $\bar{M}_r$: number of component modes in the response combination

5..3. Covariance proper transformation-based formulation

The two N-variate correlated random turbulent processes u(t), w(t) can be decomposed orthogonally using the optimum approximation from the Covariance Proper Transformation:

$$u(t) = \Theta_u x_u(t) \approx \sum_{j=1}^{\hat{N}} \theta_{uj} x_{uj}(t); \quad w(t) = \Theta_w x_w(t) \approx \sum_{j=1}^{\hat{N}} \theta_{wj} x_{wj}(t) \quad (31)$$

Putting Eq.(31) into Eq.(23) with the full-scale turbulent-induced forces in Eqs.(26a),(26b), the single-degree-of-freedom motion equation can be obtained in the time domain:

$$\ddot{\xi}_i(t) + 2\zeta_i\omega_i\dot{\xi}_i(t) + \omega_i^2\xi_i(t) = \frac{1}{2}\rho UB\left[\phi_i^T C_u \sum_{j=1}^{\hat{N}} \theta_{u_j} x_{u_j}(t) + \phi_i^T C_w \sum_{j=1}^{\hat{N}} \theta_{w_j} x_{w_j}(t) \right] \quad (32)$$

$$\ddot{\xi}_i(t) + 2\zeta_i\omega_i\dot{\xi}_i(t) + \omega_i^2\xi_i(t) = \frac{1}{2}\rho UB\left[\sum_{j=1}^{\hat{N}} A_{u_{ij}} x_{u_j}(t) + \sum_{j=1}^{\hat{N}} A_{w_{ij}} x_{w_j}(t) \right] \quad (33)$$

where $A_u = \sum_{j=1}^{\tilde{N}} A_{u_j} = \sum_{j=1}^{\tilde{N}} \phi_i^T C_u \theta_{u_j}$; $A_w = \sum_{j=1}^{\tilde{N}} A_{w_j} = \sum_{j=1}^{\tilde{N}} \phi_i^T C_w \theta_{w_j}$: cross modal factor matrices accounting

for interaction between covariance modes and structural ones; $x_u(t), x_w(t)$: covariance principal coordinates determined by Eq.(8), in such form as $x_u(t) = \{x_{u_1}(t), x_{u_2}(t),..., x_{u_N}(t)\}^T$, $x_w(t) = \{x_{w_1}(t), x_{w_2}(t),..., x_{w_N}(t)\}^T$.

Generalized response can be solved using any direct integration methods such as the fourth-order Runge-Kutta method, the Newton-β method. Finally, the globally structural responses are obtained.

5.4. Numerical example and discussions

In this application, the gust response of structures is estimated using both proper transformations with numerical example of cable-stayed bridge. Effect of the first covariance mode and the first spectral mode on the global response of structures is discussed.

A bridge has been taken for numerical example. 3D frame model is built thanks to the Finite Element Method (FEM) with total 30 nodes on bridge deck. First ten structural modes are analyzed. Damping ratio of each structural mode is assumed to be 0.005. Aerodynamic static coefficients of cross section at balanced angle ($\alpha_0 = 0^0$) and their first derivatives are experimentally determined as:

$C_L = 0.158, C_D = 0.041, C_M = 0.174, C_L' = 3.73, C_D' \approx 0, C_M' = 2.06$. Squared aerodynamic admittance functions are used the Liepmann's function as approximation of Sears' function.
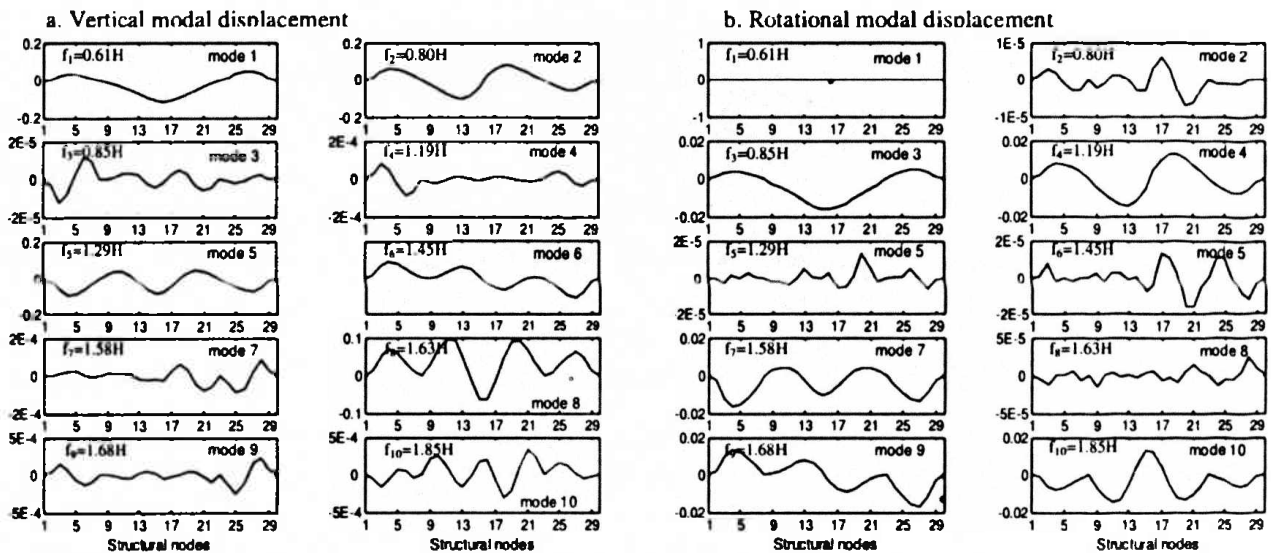

Fig. 11. Normalized structural modes: a. vertical modal displacement, b. rotational modal displacement.

Figure 11 shows the fist ten normalized structural modes associated with vertical and rotational displacements. It is observed that natural frequencies of the first ten modes vary at very low frequency band between 0.61÷1.85Hz.

In this first application, the random response of structure is predicted in the frequency domain the using the Spectral Proper Transformation. Spectral eigenvalues and spectral turbulent modes of the random turbulent fields have been computed and shown in Figures 6, Figure 7. As seen that shapes of the spectral turbulent modes of u-,w-turbulences, are unchanged during the natural frequency band. Figure 12 shows effects of number of the spectral turbulent modes (first mode, 5 modes, 10 modes and

totally 30 modes) on power spectral densities of generalized responses of vertical and rotational displacements at mid-span node 15 at mean velocity U=20m/s.

Figure 13 shows effect of number of the spectral turbulent modes on the power spectral densities of the global responses at node 15 (representative node 15 is illustrated here for a sake of brevity). As can be seen from Figure 16, there is no much different among investigated cases of cumulatively spectral turbulent modes in power spectral contribution on targeted responses. Concretely, there are no differences at resonant responses, but minor differences at background responses can be observed. It also indicates that the first spectral turbulent mode significantly and dominantly contributes on the power spectra of the global responses. Power spectra of resonant responses, moreover, can be observed at the structural modal frequencies due to influence of frequency response functions at these modal frequencies.
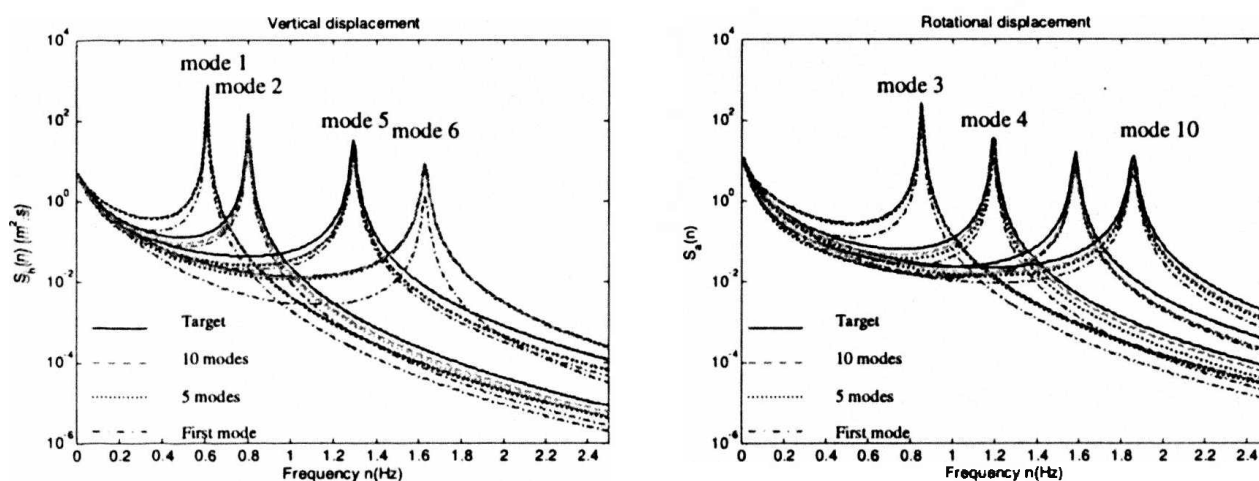

Fig. 12. Effect of number of spectral turbulent modes on power spectra of generalized responses in node 15.
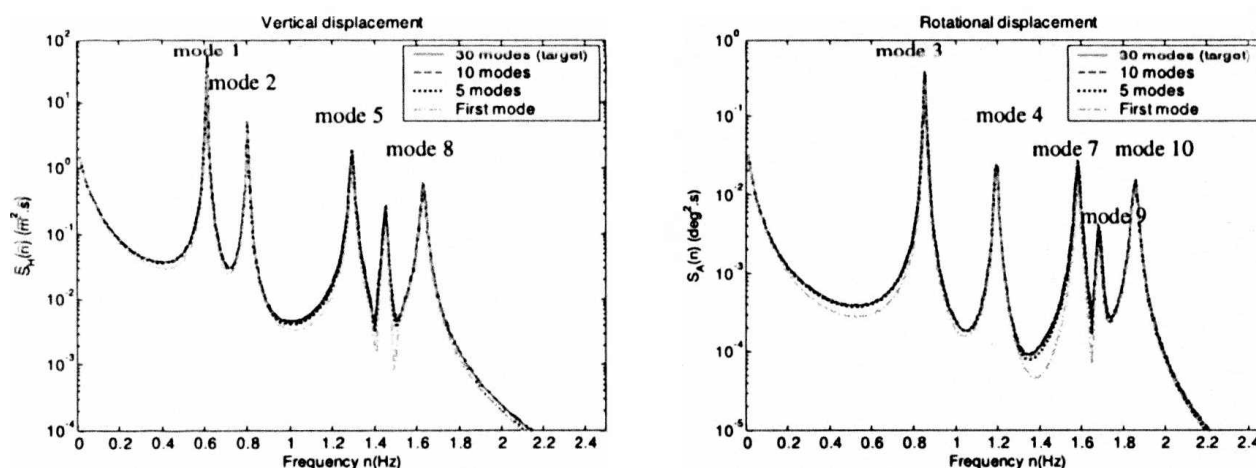

Fig. 13. Effect of number of spectral turbulent modes on power spectra of global responses in node 15.

In the second application, the response analysis is carried out in the time domain using the Covariance Proper Transformation. The time series of the turbulent wind fields u(t), w(t) have been simulated firstly using procedure mentioned in the previous part, then these simulated fields have been used to formulate the zero-time-lag covariance matrix. The covariance eigenvectors (or covariance

turbulent modes) and associated eigenvalues have been found out from the eigen solution of this covariance matrix. Turbulent fields and full-scale turbulent-induced forces are approximated optimally using the Covariance Proper Transformation to formulate the generalized response equation in the time domain.
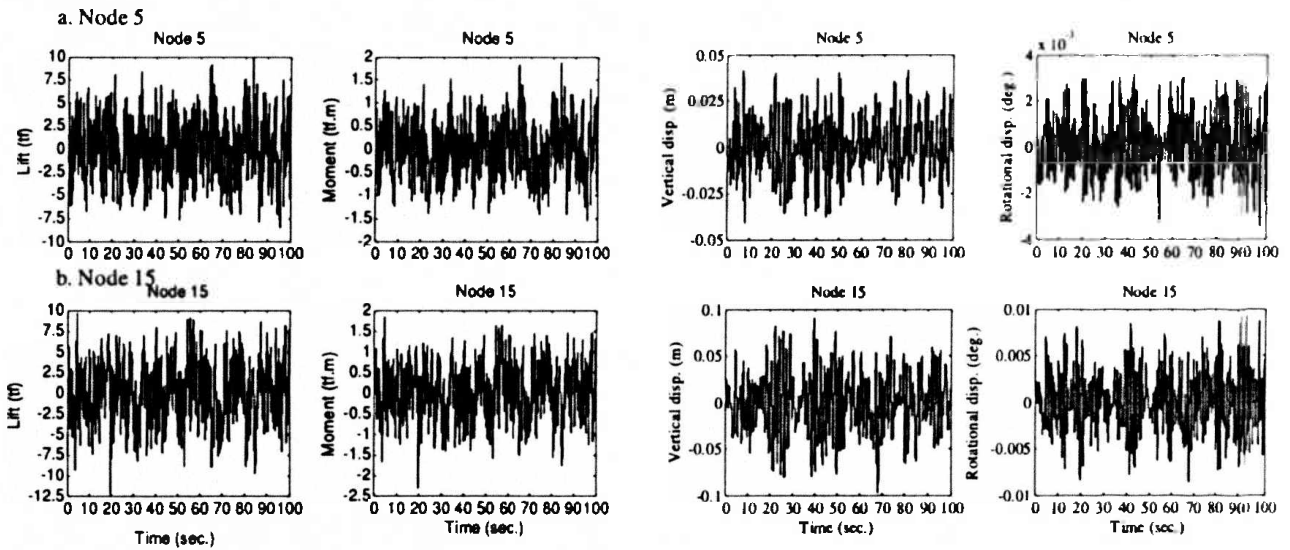

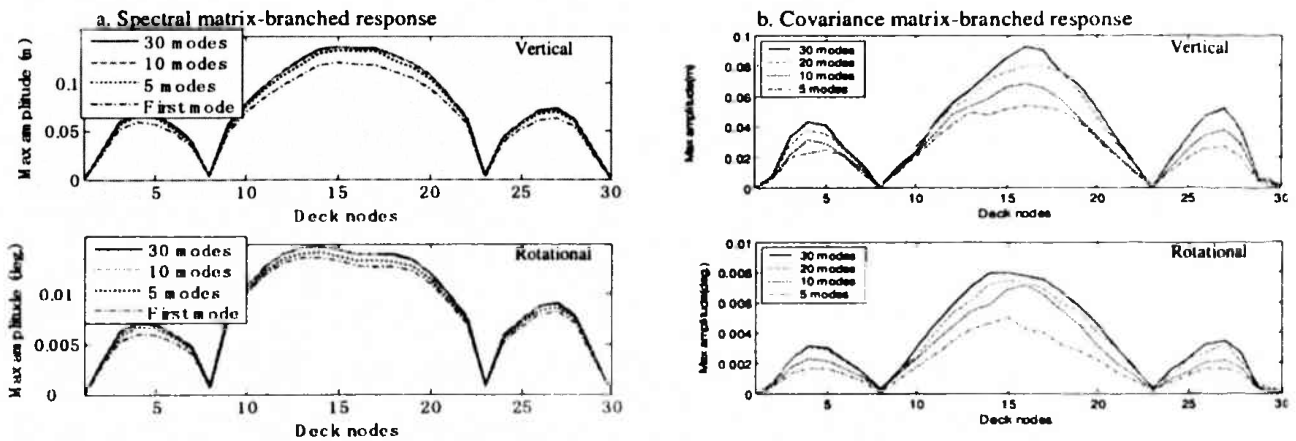Fig. 14. Time histories of global forces and global response at velocity U=20m/s: a. nodes 5, b. node 15.

Fig. 15. Global responses on deck nodes versus number of turbulent modes at U=20m/s:
a. spectral matrix-branched response, b. covariance matrix-branched response.

The Newton-β method has been used to solve Eq.(33) to compute generalized responses, before the global responses of structures can be obtained. Figure 14 shows resulted time series of global lift and global moment as well as those of globally vertical and rotational displacements in two representative nodes 5, 15 at also mean velocity U=20m/s during 100-second interval. Maximum and minimum amplitudes of responses can be determined directly from these resulted time series of responses. Figure 15 shows amplitudes of maximum vertical and rotational displacements at all bridge deck nodes at mean velocity U=20m/s in comparison between the Spectral Proper Transformation-based response (frequency-domain analysis) and the Covariance Proper Transformation-based one

(time-domain analysis) as well as to investigate effect of number of the turbulent modes on the global responses. As can be seen in Figure 15, the first turbulent mode contributes significantly on the global responses of structure in both the spectral matrix-based and covariance matrix-based responses, moreover, the first spectral turbulent mode in the frequency-domain analysis plays more important role than the first covariance turbulent one in the time-domain analysis because of its higher contribution on the global responses of structure.

6. Conclusion

Three recent advanced topics and applications of the POD and its Proper Transformations in the wind engineering have been presented here relating to (1) The analysis, synthesis and identification of the dynamic pressure field; (2) The digital simulation of the multi-variate random turbulent wind field; (3) The random response prediction of structures under the turbulent wind fields. Especially, all presented topics have been formulated and developed using both Covariance Proper Transformation in the time domain and the Spectral Proper Transformation in the frequency domain. Numerical examples have been presented for demonstrations and discussions. The turbulent wind fields, the pressure fields can be decomposed by concept of orthogonal modes either in the time domain or in the spectral one. Important role of the first covariance mode and the first spectral mode has been verified. It is observed that the first mode usually contains certain frequency peaks of hidden physical phenomena, moreover, it contributes dominantly on the field energy. Furthermore, new and comprehensive approach on the stochastic response prediction of structures in the frequency domain and in time domain has been discussed. Correlated turbulent wind fields have been represented and simplified due to either orthogonally covariance or spectral turbulent modes in which only limited number of low-order turbulent modes dominantly contributes on the random response of structures. It is also discussed that the first spectral turbulent mode plays very significant role and seems to be accuracy enough in predicting the random response of structures in the frequency domain, but more covariance turbulent modes should be required for accuracy of the random response prediction in the time domain. It is highlighted that the first spectral mode, in other words, is better than the first covariance one to analyze the random response prediction of structures.

References

[1] J.L. Lumley, *Stochastic Tools in Turbulence*, Academic Press, 1970.

[2] P. Holmes, J.L. Lumley, G. Berkooz, *Turbulence, coherent structures, dynamic systems and symmetry*, Cambridge University Press, 1996.

[3] Y.S. Li, A. Kareem, Stochastic decomposition and application to probabilistic dynamics, *J. Engrg. Mech.*, ASCE 121, 1 (1995) 162.

[4] Y.C. Liang, P. Lee, W.Z. Lim, K. Lee, C.G. Wu, Proper orthogonal decomposition and its applications – Part I: Theory, *J. Sound Vib.* 252, 3 (2002) 527.

[5] G. Berkooz, P. Holmes, L.J. Lumley, The proper orthogonal decomposition in the analysis of turbulent flows, *Annual Reviews on Fluid Mechanics* 25 (1993) 539.

[6] J.D. Holmes, Analysis and synthesis of pressure fluctuations on bluff bodies using eigenvectors, *J. Wind Eng. Ind. Aerodyn.*, 33 (1990) 219.

[7] J.D. Holmes, R. Sankaran, K.C.S. Kwok, M.J. Syme, Eigenvector modes of fluctuating pressures on low-rise building models, *J. Wind Eng. Ind. Aerodyn.*, 69-71 (1997) 697.

[8] B. Bienkiewicz, Y. Tamura, H.J. Hann, H. Ueda, K. Hibi, Proper orthogonal decomposition and reconstruction of multi-channel roof pressure, *J. Wind Eng. Ind.Aerodyn.*, 54-55 (1995) 369.

[9] H. Kikuchi, Y. Tamura, H. Ueda, K. Hibi, Dynamic wind pressure acting on a tall building model – proper orthogonal decomposition, *J. Wind Eng. Ind. Aerodyn.*, 69-71 (1997) 631.

[10] Y. Tamura, S. Suganuma, H. Kikuchi, K. Hibi, Proper orthogonal decomposition of random wind pressure field, *J. Fluid Struct.*, 13 (1999), 1069.

[11] Shinozuka, M., Yun, C.M., Seya, H., Stochastic methods in wind engineering, *J. Wind Eng. Ind. Aerodyn.*, 36 (1990) 829.

[12] Di Paola, M, Gullo, I., Digital generation of multi-variate wind field processes, *J. Prob. Eng. Mech.*, 16 (2001) 1.

[13] Tubino, F., Solari, G., Double proper transformation for representing and simulating turbulence field, *J. Eng. Mech.*, ASCE 131, 12 (2005) 1302.

[14] Le, T.H, Nguyen, D.A., Digital simulation of turbulent field and gust response analysis of line-like structures based on proper orthogonal decomposition, *Proc. Int'l Conf. on Nonlinear Analysis and Engineering Mechanics Today (NA-EMT2006)*, Ho Chi Minh City, Vietnam.

[15] Solari, G., Carassale, L., Modal transformation tools in structural dynamics and wind engineering, *Wind & Structures*, 3, 4 (2000) 221.

[16] Chen, X., Kareem, A., Proper orthogonal decomposition-based modeling, analysis, and simulation of dynamic wind load effects on structures", *J.Engrg. Mech.*, ASCE 131, 4 (2005) 325.

[17] Solari, G., Tubino, F., Gust response of long span bridges by double modal transformation, *Proc. 4th European and African Conference on Wind Engineering (EACWE4)* 2005.

[18] Matsumoto, M., Le, T.H., Time and frequency gust response prediction of bridges using proper orthogonal decomposition, *Proc. of the Int'l Conference on Wind Engineering (ICWE12)*, Cairns Australia 2007.

[19] De Grenet, E.T., Ricciardelli, F., Spectral proper transformation of wind pressure fluctuations: application to a square cylinder and a bridge deck, *J. Wind Eng.Ind. Aerodyn.*, 92 (2004) 1281.

[20] Cao, Y.H., Xiang, H.F., Zhou, Y., Simulation of stochastic wind velocity field on long-span bridges, *J. Eng. Mech.*, ASCE 126, 1 (2000) 1.

[21] Shinozuka, M., Jan, C.M., Digital simulation of random processes and its application, *J. Sound Vib.*, 25, 10 (1972) 111.

[22] Simiu, E., Scanlan, R.H., *Wind Effects on Structures*, John Wiley&Sons, 1986.